

Elucidating Meta-Structures of Noisy Labels in Semantic Segmentation by Deep Neural Networks

Yaoru Luo, Guole Liu, Yuanhao Guo, and Ge Yang

Abstract— The supervised training of deep neural networks (DNNs) by noisy labels has been studied extensively in image classification but much less in image segmentation. So far, our understanding of the learning behavior of DNNs trained by noisy segmentation labels remains limited. In this study, we address this deficiency in both binary segmentation of biological microscopy images and multi-class segmentation of natural images. We classify segmentation labels according to their noise transition matrices (NTM) and compare performance of DNNs trained by different types of labels. When we randomly sample a small fraction (e.g., 10%) or flipping a large fraction (e.g., 90%) of the ground-truth labels to train DNNs, their segmentation performance remains largely the same. This indicates that *DNNs learn structures hidden in labels rather than pixel-level labels per se in their supervised training for semantic segmentation*. We call these hidden structures “meta-structures”. When we use labels with different perturbations to the meta-structures to train DNNs, their performance in feature extraction and segmentation degrades consistently. In contrast, addition of meta-structure information substantially improves performance of an unsupervised model in binary semantic segmentation. We formulate meta-structures mathematically as spatial density distributions and quantify semantic information of different types of labels, which we find to correlate strongly with ranks of their NTM. We show theoretically and experimentally how this formulation explains key observed learning behavior of DNNs.

Index Terms— Semantic segmentation, meta-structure, noisy label, spatial density distribution

1 INTRODUCTION

Deep neural networks (DNNs) have achieved remarkable success in challenging image segmentation tasks [1-3]. However, their supervised training requires pixel-level labels. Manual annotation of pixels is laborious. More importantly, it introduces label noise, especially in border regions of image objects. Despite that label noise is generally more common in image segmentation than image classification, studies on the training of DNNs by noisy labels so far have focused largely on classification. Is it really necessary to accurately label each pixel of training images? How will segmentation performance of DNNs be influenced by different types of label noise? Answering these questions is critical to understanding the role of labels in training of DNNs. It will also provide important insights into the learning behavior of DNNs.

Different types of noisy labels have been used to study the learning behavior of DNNs in image classification, especially partially corrupted or randomly shuffled labels [4, 5]. In image segmentation, there are image-level and pixel-level label noise. Image-level label noise refers to erroneous

TABLE 1 DIFFERENT TYPES OF SEGMENTATION LABELS

Labels	Meaning	Description	Accurate Boundary?	Randomized Labels?
CL	Clean Label	Ground truth labels	Yes	No
RCL	Randomized Clean Label	Randomly sampled or flipped pixel labels from ground truth	Yes	Yes
PCL	Perturbed Clean Label	Dilation/erosion/skeleton of ground truth	No	No
RL	Random Label	Randomly generated pixel labels	No	Yes

semantic annotation of image objects, whereas pixel-level label noise refers to erroneous semantic annotation of image pixels. We focus on pixel-level label noise in this study.

Specifically, we examine the performance of DNNs trained by four different types of labels, summarized in Table 1 and illustrated in Figure 1. To quantitatively characterize the segmentation performance of DNNs trained by these labels, we experiment on two representative segmentation models, U-Net [6] and DeepLabv3+ [7], using the same loss function (binary cross-entropy) and optimizer (stochastic gradient descent, SGD). Performance of DNNs trained by the labels ranks from the best to the worst as follows:

• The authors are with the School of Artificial Intelligence, University of Chinese Academy of Sciences and the National Laboratory of Pattern Recognition, Institute of Automation, Chinese Academy of Sciences. E-mail: {luoyaoru2019, yuanhao.guo}@ia.ac.cn, {ge.yang, liuguole}@ucas.edu.cn.

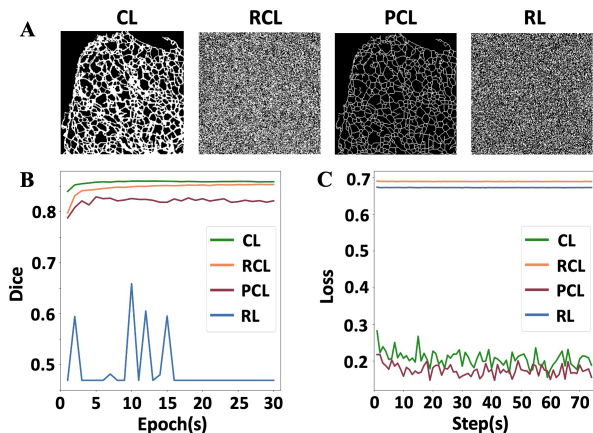


Fig. 1. Segmentation performance of DNNs trained by different types of labels. (A) Four types of training labels for an image of the endoplasmic reticulum from the ER dataset [8]. CL: ground truth from manual annotation. RCL: each pixel label in CL is randomly flipped with a probability of 0.45. PCL: Skeleton of CL. RL: each pixel is randomly labeled as 1, i.e. foreground, with a probability of 0.5. (B) Testing dice scores during training. (C) Training loss of each optimization step.

$$CL \approx RCL > PCL > RL. \quad (1)$$

As shown in Figure 1, when U-Net is trained with for example 45% of the labels randomly flipped (i.e., RCL) in binary segmentation, its performance remains largely the same as trained by the original ground truth (CL). Similar results are obtained on DeepLabv3+ (see Appendix A). These results indicate that DNNs learn structures hidden in the noisy labels rather than the pixel labels *per se* in their training for segmentation. We name these hidden structures "meta-structures".

Similar as observed in image classification in [5], we find that DNNs memorize random labels in segmentation because the training loss under RCL and RL quickly converges to a constant but not under CL and PCL (Figure 1C). Meanwhile, similar as observed in image classification in [4], we find that before memorizing RL, DNNs prioritize learning real patterns in labels because the dice score (Figure 1B, blue line) first fluctuates greatly then quickly drops to a low level. Motivated by the fact that RL requires no manual annotation, we develop a direct application of meta-structures in unsupervised learning for binary segmentation. Specifically, we develop a DNN model that sets RL as the initial training label and iteratively transits from RL to RCL by adding meta-structure information.

Main Contributions

The main research contributions of this study are as follows:

1. We provide direct experimental evidence that DNNs learn implicit structures hidden in noisy labels in semantic segmentation (Section 4). We refer to these implicit structures as meta-structures and model them mathematically as spatial density distributions. We show theoretically and experimentally that this model explains observed learning

behavior of DNNs and that it quantifies semantic information in different segmentation labels (Section 7).

2. We have identified some fundamental properties of meta-structures and, therefore, noisy labels. We find that DNNs trained with labels under different perturbations to their meta-structures exhibit different yet consistently worse performance in feature extraction and segmentation (Section 5).

3. We demonstrate how to use meta-structure information in semantic segmentation. Specifically, by utilizing meta-structure information, we have developed an unsupervised model for binary segmentation that outperforms state-of-the-art unsupervised models and achieves remarkably competitive performance against supervised models (Section 6).

2 RELATED WORK

Generalization Capability of Models Trained by Noisy Labels in Image Classification. Previous studies have shown that DNNs can be trained to memorize large volumes of randomized labels but with poor generalization capability [5] and that they prioritize learning patterns of noisy labels before memorization [4]. These phenomena contradict traditional statistical learning theory [9] and attract a lot of research interest to characterize the generalization capability of DNNs trained by noisy labels. For example, it is shown empirically that generalization accuracy can be quantitatively characterized in terms of noise ratio in datasets [10]. Upper bounds on generalization errors are also derived in terms of mutual information between input and output [11]. Furthermore, the information memorized by DNNs is quantified using Shannon mutual information between weights and labels [12]. However, the focus of these studies is on image classification. In this study, we examine the generalization of DNNs trained by different noisy labels in semantic segmentation.

Training with Noisy Labels. In image classification, two types of methods are commonly used to deal with noisy labels, including data cleansing and noise-tolerant enhancement. Data cleansing, which aims to filter out training labels that appear to be erroneous, reassigns labels by using alpha blending of given noisy labels [13] or corrects labels using an ensemble of networks [14]. Suspicious labels can also be picked and sent to a human annotator for correction [15]. Noise-tolerant enhancement, which aims to increase the robustness of learning systems under noisy training process, includes developing noise-robust loss functions [16-22], designing custom architectures based on e.g., co-teaching [23, 24], and utilizing multi-tasks frameworks to infer true labels [25-27]. Although most of these methods performed well in image classification tasks, their performance in image segmentation is unknown.

Unlike in image classification, much fewer studies on semantic segmentation focus on noisy labels. Min and coworkers proposed to weaken the influence of back-propagated gradients caused by incorrect labels based on mutual attention [28]. Shu and coworkers proposed to leverage local visual cues to automatically correct label errors [29]. Semi-supervised or unsupervised methods are also

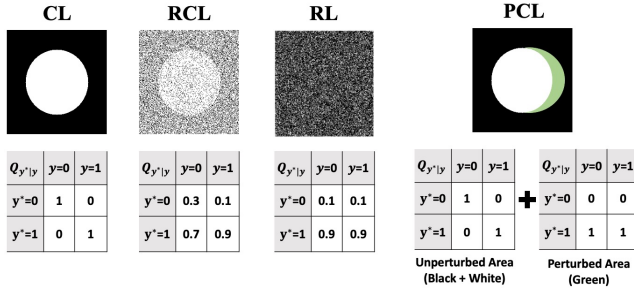


Fig. 2. Examples of different types of binary semantic labels represented by their noise transition matrices (NTM).

proposed [30-33]. Although these studies improved the generalization ability of DNNs trained with noisy labels, an in-depth understanding of the fundamental roles of labels in training remains lacking.

Unsupervised Segmentation. Some studies try to segment images by learning pixel representation in a self-supervised setting [34, 35]. However, the proposed methods still relied on initialization from other annotated datasets. A small number of studies address image segmentation in a fully unsupervised way. For example, methods have been proposed to maximize the mutual information between augmented views [36, 37]. A DNN architecture consisting of convolutional filters for feature extraction and differentiable processes for feature clustering has also been proposed [38]. Overall, however, performance of unsupervised segmentation methods remains to be further improved.

3 METHOD

3.1 Definitions of different Labels

We define the four types of labels listed in Table 1 as follows:

CL: Clean labels (CLs) are ground-truth labels. They have accurate boundaries and non-randomized pixel labels.

RCL: Randomized clean labels (RCLs) are generated by randomly sampling or flipping pixel labels in CLs. For multi-class labels, a fraction of true pixel labels is randomly swapped with randomly selected labels from other classes. RCLs have accurate boundaries but randomized pixel labels. See Figure 4 for examples of randomized binary labels and multi-class labels.

PCL: Perturbed clean labels (PCLs) are generated by dilation, erosion, or skeletonization of regions of CLs. They have inaccurate object boundaries but non-randomized pixel labels. Examples of PCL are shown in Figure 7.

RL: Random labels (RLs) are generated by randomly assigning pixel labels with a certain probability. They can be considered as a strong perturbation of CLs because they contain no information from CLs. RLs have inaccurate boundaries and randomized pixel labels. Examples of RL are shown in Figure 9.

3.2 Representing Labels by Noise Transition Matrix

Let (X, Y) denote the input image $X \in R^{H \times W}$ with

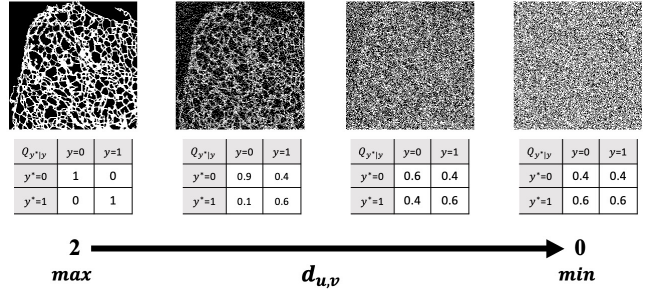


Fig. 3. Examples of different labels generated with different NTM. The entropy of pixel-level labels is gradually increasing from CL (left) to RL (right), as with decreasing of chaotic distance $d_{u,v}$ from maximum (2) to minimum (0).

associated hidden uncorrupted label $Y \in R^{H \times W}$, where H and W denote the height and width of the images, respectively. In Y , each pixel label y is correctly annotated by labels from a semantic class set $\{1, 2, \dots, M\}$. Based on class-conditional classification noise process (CNP) [39] that assuming correct labels will be independently corrupted to other classes, we use $p(y^* = j | y = i)$ to denote the probability of flipping pixel label y in class i to the noisy pixel label y^* in class j . We abbreviate flipping probability $p(y^* = j | y = i)$ as $p_{j|i}$ and the NTM $Q_{y^*|y}$ of labels can be conducted as a $M \times M$ matrix according to $p_{j|i}$.

Thus, CL can be synthesized by flipping Y with an identity matrix. RCL can be synthesized by flipping Y with an arbitrary $Q_{y^*|y}$ whose rank of $Q_{y^*|y}$ ranges from $(1, M]$. PCL can be synthesized by flipping Y with a series of $Q_{y^*|y}$. Within unperturbed areas, $Q_{y^*|y}$ is an identity matrix. Within perturbed areas, the rank of $Q_{y^*|y}$ equals 1 and all elements are 1 in a certain row. RL can be synthesized by flipping Y with arbitrary $Q_{y^*|y}$ whose rank equals 1. Examples of these four types of labels and their $Q_{y^*|y}$ are shown in Fig.2.

3.3 Chaotic Distance

We define a distance $d_{u,v}$, which we refer to as chaotic distance, to measure the pixel-level entropy between class u and class v :

$$d_{u,v} = \|p_{k|u}, p_{k|v}\|_1 = \sum_{k=1}^M |p_{k|u} - p_{k|v}|, \quad (2)$$

where M denotes the number of classes. $p_{k|u}$ and $p_{k|v}$ are the probabilities in column $y = u$ and $y = v$ of NTM $Q_{y^*|y}$, respectively. $\|\cdot\|_1$ is L1 norm. As shown in Fig.3, the maximum of chaotic distance $d_{u,v} = 2$, indicating pixel noisy-free between two classes. With decreasing $d_{u,v}$, the entropy of pixel-level labels between two classes gradually increases until reach the maximum entropy (i.e., randomization) when $d_{u,v} = 0$.

3.4 Datasets and Experiment Configurations

We use two public fluorescence microscopy image datasets for binary-class semantic segmentation, including

TABLE 2
PERFORMANCE OF CL AND RCL ON ER DATASETS

Training Labels	Noise Ratio	Dice (%)
CL	0	85.9
RCL	$P_{sample} = 0.1$	85.5
	$P_{sample} = 0.3$	85.6
	$P_{sample} = 0.5$	85.8
	$P_{flip} = 0.2$	85.9
	$P_{flip} = 0.4$	85.5
	$P_{flip} = 0.45$	85.2

TABLE 3
PERFORMANCE OF CL AND RCL ON CITYSCAPES DATASETS

Training Labels	Noise Ratio	IoU (%)
CL	0	64.8
RCL	$P_{sample} = 0.1$	64.6
	$P_{sample} = 0.3$	64.5
	$P_{sample} = 0.5$	64.8
	$P_{flip} = 0.2$	64.7
	$P_{flip} = 0.4$	64.6
	$P_{flip} = 0.45$	64.7

endoplasmic reticulum (ER) and mitochondria (MITO) [8]. We use Cityscapes [40] dataset, which includes 19 urban scene classes, for multi-class semantic segmentation.

To simplify the theoretical analysis of multi-class labels, we build another dataset which choose a subset of Cityscapes that contains 3 of the 19 classes in Cityscapes, including classes of road, sidewalk and vegetation. We refer to this customized dataset as Cityscapes-3. Detailed statistics and samples of four datasets are shown in Appendix B.

We choose U-Net [6] for binary-class semantic segmentation because it is widely used in biomedical image segmentation. We choose DeepLabv3+ [7] for multi-class semantic segmentation because it is a benchmark model for natural image segmentation. We use different hyperparameters (e.g., learning rate and weight decay) for training U-Net on different noisy labels, please see details in Appendix B.3. We train DeepLabv3+ with the common setting: learning rate 0.01; weight decay 0.0001 and momentum 0.01. All models are optimized by Stochastic Gradient Descent (SGD) with cross-entropy loss function on a Dell PowerEdge T640 server with 4 NVIDIA 2080Ti GPUs. Dice score and intersection over union (IoU) are used to measure performance for binary-class and multi-class datasets, respectively.

4 EXPERIMENTAL EVIDENCE FOR EXISTENCE OF META-STRUCTURES

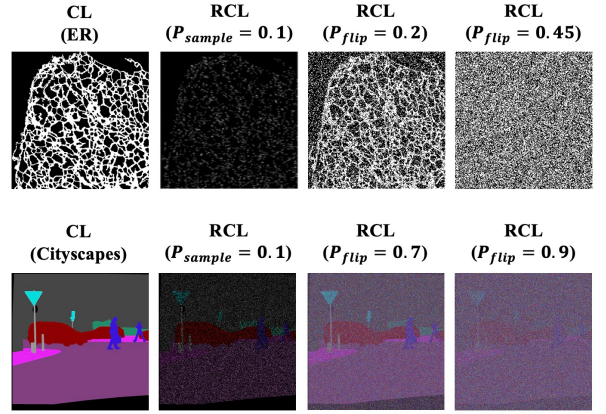


Figure 4. Examples of RCL synthesized by random sampling/flipping with different probability (P_{sample}/P_{flip}).

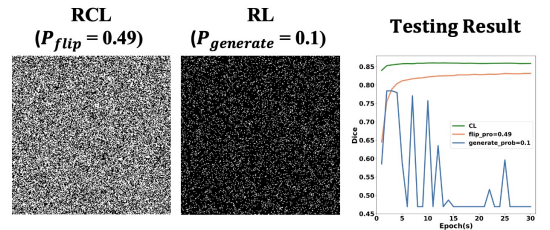


Figure 5. Comparing training performance of RCL versus RL. Testing dice score of DNNs trained by CL, RCL ($P_{flip} = 0.49$) and RL ($P_{generate} = 0.1$).

In this section, we examine the learning behavior of DNNs trained by CL and RCL in both binary-class and multi-class segmentation.

4.1 Existence of Meta-Structures

As shown in Fig. 4, we synthesized a series of RCL with different flipping probabilities P_{flip} on binary-class dataset (ER) and multi-class dataset (Cityscapes), respectively. Note that random sampling is a specific form of random flipping that swaps non-background pixel labels to background with probability $1 - P_{sample}$.

Table 2 shows the segmentation results of U-Net trained by ER dataset. The final Dice scores decrease only slightly and the maximum gap between final Dice scores of CL and RCL is 0.7%. Table 3 shows the segmentation results of DeepLabv3+ trained by Cityscapes dataset. No degradation in segmentation performance measured in IoU is observed.

Taking the results together, we reason that semantic information contained in CL is completely or largely preserved in RCL.

4.2 Meta-Structures vs. Pixel-level labels

So far, we have shown that DNNs can learn segmentation from extremely noisy labels. However, it is unclear whether meta-structures or pixel-level labels contribute more to segmentation performance. For example, in binary-class segmentation when $P_{flip} \leq 0.49$, the fraction of correctly annotated pixels ($\geq 51\%$) still exceeds the fraction of incorrectly annotated pixels ($\leq 49\%$). This raises the possibility that DNNs learn from the majority of correct pixel-level labels rather than meta-structures.

TABLE 4
SEGMENTATION PERFORMANCE ON ER DATASET

$1 - P_{0 1} \pm \varepsilon$		$P_{0 1}$			
		0.2	0.4	0.6	0.8
- ε	$\varepsilon \geq 0.1$	EQ	EQ	EQ	EQ
	$\varepsilon = 0.05$	-0.6%	-0.7%	-0.9%	-0.7%
	$\varepsilon = 0.01$	-3.7%	-2.8%	-3.1%	-2.4%
$\varepsilon = 0$		OF	OF	OF	OF
+ ε	$\varepsilon = 0.01$	-3.3%	-3.9%	-3.0%	-2.9%
	$\varepsilon = 0.05$	-0.7%	-0.6%	-0.7%	-0.9%
	$\varepsilon \geq 0.1$	EQ	EQ	EQ	EQ
Baseline (Dice)		85.9%			

* EQ: EQUALITY. OF: OVERFITTING

TABLE 5
SEGMENTATION PERFORMANCE ON CITYSCAPES-3 DATASET

Labels	Rank	$Q_{y^* y}$	Minimum $d_{u,v}$	IoU (%)
CL	3	1 0 0	$d_{arbitrary} = 2$	94.3 (Baseline)
		0 1 0		
		0 0 1		
RCL	3	0.5 0.3 0.2	$d_{1,3} = 0.6$	93.8 (-0.5)
		0.2 0.6 0.2		
		0.3 0.1 0.6		
	3	0.4 0.3 0.3	$d_{arbitrary} = 0.2$	92.9 (-1.4)
		0.3 0.4 0.3		
		0.3 0.3 0.4		
	2	0.6 0.3 0.3	$d_{2,3} = 0$	39.2 (-55.1)
		0.1 0.6 0.6		
		0.3 0.1 0.1		
	2	0.2 0.3 0.2	$d_{1,3} = 0$	36.9 (-57.4)
		0.1 0.5 0.1		
		0.7 0.2 0.7		
1	0.4 0.4 0.4	$d_{arbitrary} = 0$	OF	
	0.3 0.3 0.3			
	0.3 0.3 0.3			
1	0.1 0.1 0.1	$d_{arbitrary} = 0$	OF	
	0.2 0.2 0.2			
	0.7 0.7 0.7			

* $d_{arbitrary}$ DENOTES CHAOTIC DISTANCE BETWEEN ARBITRARY TWO CLASSES. OF: OVERFITTING

To test this possibility, we generate entirely random labels, referred to as RL on ER dataset. Each pixel is randomly assigned to foreground with a certain generation probability. Sample image is shown in Figure 5. Here, we set the generation probability as 0.1 and compare with the noisy label synthesized by random flipping with a probability $P_{flip} = 0.49$. While the randomly flipped labels still contain the meta-structures, the randomly generated labels do not. When we count the number of correctly annotated pixels using CL as the reference, we find that the pixel-level error rate of the randomly generated labels is around 31%, which is much lower than the error rate of randomly flipped labels (49%). If DNNs mainly learn from the pixel-level labels, the segmentation performance trained by RL would be better than the randomly flipped labels.

However, segmentation performance of U-Net trained by RL is actually worse than randomly flipped labels (Fig.5). This result further supports that DNNs learn from

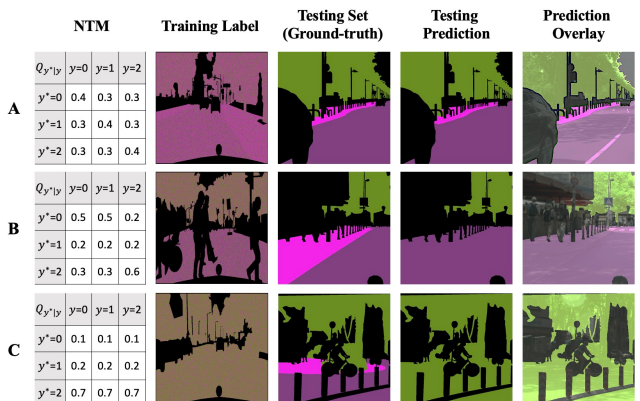


Fig. 6. Segmentation results of DeepLabv3+ trained by different labels on Cityscapes-3 dataset. The segmented classes reduce with decreasing the rank of NTM.

meta-structures in labels rather than pixel-level labels per se in their supervised training for semantic segmentation.

4.3 Negative Correlation between Segmentation Performance and Chaotic Disance

By using chaotic distance to quantify entropy of pixel-level labels, we further explore the relationship between segmentation performance and chaotic distance.

Binary-class Semantic Segmentation. Based on $Q_{y^*|y} = \begin{bmatrix} 1 - P_{1|0} & P_{0|1} \\ P_{1|0} & 1 - P_{0|1} \end{bmatrix}$, we synthesized a series of RCL by different probability pairs ($P_{0|1}, P_{1|0} = 1 - P_{0|1} \pm \varepsilon$), where $\varepsilon > 0$ and $P_{0|1} \in \{0.2, 0.4, 0.6, 0.8\}$. The chaotic distance of all RCL equals 2ε . We use the result of CL as the baseline. For the results of RCL, we show decreasing value when compared to the baseline.

Table 4 shows the results of U-Net trained on ER dataset. We can clearly see the negative correlation between segmentation performance and chaotic distance. Specifically, at each probability pair ($P_{0|1}, P_{1|0}$) when $d = 0$, the model is overfitting. However, even when d is slightly larger than 0, e.g., $d = 0.02$ when $Q_{y^*|y} = \begin{bmatrix} 0.89 & 0.9 \\ 0.11 & 0.1 \end{bmatrix}$, the model surprisingly achieves competitive performance compared to baseline and the largest degradation of Dice scores is within 5%. Moreover, with slightly increasing $\varepsilon = 0.05$ ($d = 0.1$), the performance quickly recovery at the similar level as the baseline. When $\varepsilon \geq 0.1$ ($d \geq 0.2$), the performance trained by RCL is equal to the performance trained by CL.

Consistent results on MITO dataset are shown in Appendix C.1. In summary, for most situations when $d \neq 0$, DNNs have strong robustness to pixel-level noises. As $d \rightarrow 0$ the segmentation performance of DNNs decreases, and DNNs become overfitting when $d = 0$.

Multi-class Semantic Segmentation. To simplify visualize the results on multi-class semantic segmentation, we experiment on Cityscapes-3 that labels only contain three semantic classes. We synthesize RCL with different 3×3 $Q_{y^*|y}$. We train DeepLabv3+ and the results are shown in Table 5.

As we can see, when RCL (i.e., Rank=3) that minimum

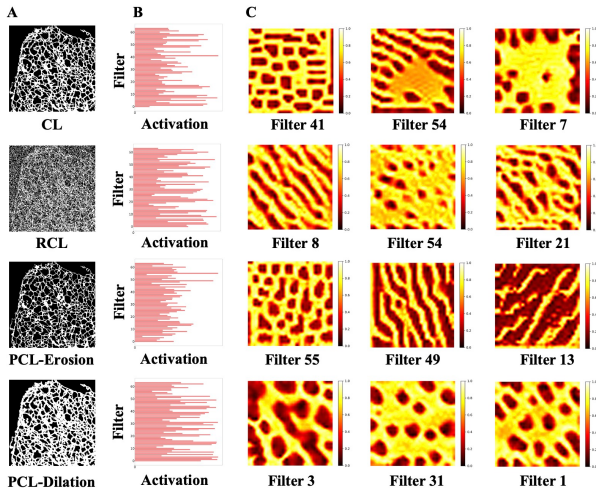


Fig. 7. Feature patterns generated by different pre-trained DNNs. A: Different types of labels for training DNNs. B: Activation values of filters in the penultimate layer. C: Pattern images generated by top-3 filters according to Algorithm 1.

$d > 0$, the segmentation performance of DNNs is similar to DNNs trained by CL. All three semantic classes can be correctly segmented as shown in Fig.6A.

When RCL (i.e., Rank=2) exists certain two classes that minimum $d = 0$, indicating at least two semantic classes are randomized, the segmentation performance of DNNs drops sharply and cannot distinguish the corresponding classes. The visualization results are shown in Fig.6B.

When RCL (i.e., Rank=1) that $d = 0$ for arbitrary two classes, indicating all semantic classes are randomized, DNNs are overfitting. Fig.6C shows the segmentation results.

Overall, the results of multi-class semantic segmentation are consistency with the results of binary-class semantic segmentation.

4.4 Summary

Although RCL are uncommon in real-world applications, it allowed us to discover counterintuitive learning behavior that DNNs learn meta-structure rather than pixel-level labels per se in segmentation. Specifically, section 4.1 and 4.2 show that:

DNNs trained by randomized labels that contain similar meta-structure information as the ground truth labels provide similar performance in semantic segmentation.

Furthermore, since chaotic distance $d = 0$ will lead decreasing of rank in $\mathcal{Q}_{y^*|y}$, based on the experiments in section 4.3, we find that:

The decreasing of rank in $\mathcal{Q}_{y^|y}$ will lead to semantic disappearing in labels.*

Mathematical formulation and proof of these findings are presented later in section 7.

5 FURTHER CHARACTERIZATION OF META-STRUCTURES

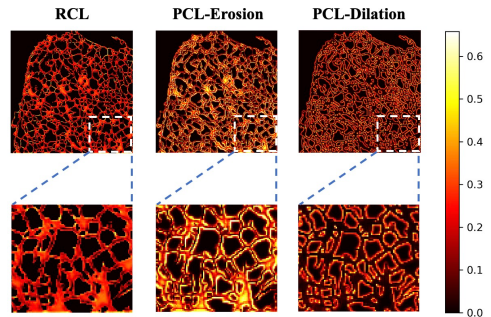


Fig. 8. Difference images of prediction map between CL and PCL.

In this section, we further characterize the properties of meta-structures by analyzing PCL and RL.

5.1 Learning Behavior of DNNs Trained by PCL

Inaccurate object boundaries are a common source of label noise in image segmentation. We simulate inaccurate boundaries using dilation and erosion of CL, which we refer to as PCL (Table 1). We explore the characteristics of PCL in the following two aspects: feature patterns and segmented images. The visualization samples of PCL are shown in Fig.7A.

Feature Patterns. To elucidate how PCL affects the feature extraction of DNNs, we generate the feature patterns that DNNs prioritize recognizing.

The basic idea is that a pattern to which the filter is responding maximally could be a good first-order representation [41]. Based on this, we first feed an identical image I into DNNs which are pre-trained by different labels, i.e., CL, RCL and PCL. Then we find hidden filters that have the highest activations in the penultimate layer (i.e., before the softmax layer). This helps us find out the optimal filters for representing the input image I . Next, we use SGD to backwardly synthesize the pattern images that can maximize activate the selected filters by inputting a random image X . If noisy labels (e.g., PCL) don't perturb the feature extraction of DNNs, the generated pattern images should be consistent with the pattern images which synthesized by DNNs trained by CL. The whole procedure is shown in Algorithm 1.

We experiment on ER dataset since the low-level features of endoplasmic reticulum are easily distinguished, i.e, tubule structures and sheet structures. We pre-train U-Net by four types of labels as shown in Fig.7A, including CL, RCL, eroded PCL and dilated PCL. Fig.7B shows the activation of hidden filters in the penultimate layer (64 filters in total). Fig.7C shows the pattern images generated by the top three filters.

As we can see, for CL and RCL, the pattern images include both tubule structures and sheet structures of endoplasmic reticulum. However, for eroded PCL, the tubule structures are slender and lack sheet objects. For dilated PCL, the tubules as thicker as sheet structures. Thus, training DNNs with PCL will bias the feature extraction.

Algorithm 1 Pattern Synthesis Strategy

Require: random image X , Input image I , pre-trained model \mathcal{F} , hidden filter f , number of layers l , iteration steps n .

- 1: $f = \operatorname{argmax} \mathcal{F}^{l-1}(I)$
- 2: **while** $t < n$ **do**
- 3: $\min \mathcal{L} = -f(X_t)$
- 3: $X_{t+1} = X_t - \eta \nabla_X \mathcal{L}$
- 4: $t = t + 1$
- 5: **end while**

Segmented Images. We calculate the absolute difference image between the prediction map trained by CL and the prediction map trained by noisy labels. The difference image of RCL, eroded PCL and dilated PCL are shown in Fig. 8.

As we can see, for the difference image of RCL, similar values are uniformly distributed on semantic objects, indicating we can reach the same segmented images after selecting appropriate thresholds for both CL and RCL. However, for eroded PCL and dilated PCL, the difference-images have structural deficiencies in semantic objects which cannot rectify segmented images by thresholding. Table 6 shows the segmentation results of U-Net trained by PCL on ER datasets and we find consistence degradation of performance. Thus, PCL will bias the final segmented images.

5.2 Learning Behavior of DNNs Trained by RL

Zhang *et al.* [5] and Arpit *et al.* [4] have shown that DNNs learn simple patterns before fitting RL by memorization. This conclusion, however, is drawn in image classification. In our study, we investigate whether DNNs exhibit similar behavior in image segmentation. We generate RL under different generation probabilities (Figure 9) from 0 to 0.5. We experiment on ER dataset and show the results of U-Net in Figure 9.

From the testing results on ER dataset (Figure 9, lower left panel), we find that the learning process consists of two stages. In the first stage, the dice scores fluctuate substantially and reach several high values, indicating that the U-Net keeps learning and is not yet strongly influenced by RL. In the second stage, the dice scores drop quickly then converge to a low value, indicating that the U-Net start memorizing as the generalization ability becomes worse. Meanwhile, we find that under a higher generation probability, the training loss converges more quickly (Figure 9, right panel), indicating DNNs have a higher tendency to memorize. Similar results are observed on DeepLabv3+. See Appendix C.2 for further details. Overall, the learning behavior of DNNs trained by RL in segmentation is consistent with the learning behavior of DNNs trained by RL in classification.

5.3 Conclusion

Compared to CL and RCL, the PCL and RL contain different perturbations to meta-structures. We observe consistent degradation in segmentation performance and conclude that:

Training of DNNs by labels with progressively stronger perturbation to the meta-structure exhibit progressively worse

TABLE 6
SEGMENTATION PERFORMANCE OF PCL ON BINARY-CLASS DATASETS

Dataset	Training Labels	Dice (%)
ER	CL	85.8
	PCL-Erosion	83.7
	PCL-Dilation	83.8

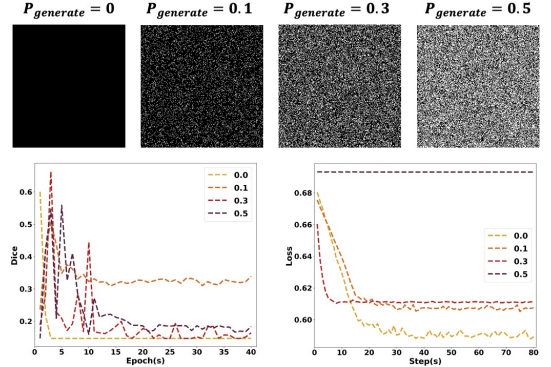


Fig. 9. Testing dice score (left) and training loss (right) trained by RL.

segmentation performance

Mathematical formulation and proof of this argument is presented later in section 7.

6 UNSUPERVISED BINARY-CLASS SEGMENTATION BASED ON META-STRUCTURES

Here we propose an unsupervised segmentation method which without using any annotated labels for binary-class images. The basic idea behind our method is that DNNs can reach good segmentation performance even if trained by RL in early training steps. This provides a chance for us to transfer the arbitrary RL to RCL by iteratively incorporating the structure information.

We name our model as iterative ground truth training (iGTT). Although iGTT is highly customized for binary-class segmentation, our goal is to provide an example of utilizing meta-structures in practice.

6.1 Notation

Given data pair $(X, Y) \in \mathbb{R}^{H \times W}$, where X denotes the input image, Y denotes the binary-class labels with foreground and background labeled as 1 and 0, respectively. H and W denote image height and width, respectively. For iGTT, we use U-Net as the base model and only output the probability that belongs to the foreground for each pixel. The output image is denoted as P .

6.2 Unsupervised Iteration Strategy

We use fully black images to initialize the labels Y^* then iteratively update it in following epochs. Specifically, for the n_{th} epoch, we first update the model parameters θ based on current epoch labels Y^* . Then we directly thresholding

TABLE 7

SEGMENTATION PERFORMANCE OF DIFFERENT MODELS

Training	Model	DICE	AUC	ACC
Supervised	U-Net	85.9	97.0	91.0
	HRNet	86.0	97.1	91.1
	DeepLabv3+	81.6	94.8	87.6
Unsupervised	AGT	76.2	82.6	85.1
	Otsu	69.4	76.7	84.7
	DFC	78.1	85.2	84.4
	AC	73.1	87.8	81.4
	iGTT (w EMS)	78.8 _{1.17}	91.6 _{1.04}	85.4 _{1.06}
	iGTT (w/o EMS)	73.9 _{0.97}	84.5 _{2.52}	81.1 _{1.03}

* NUMBERS IN SUBSCRIPTS REPRESENT STANDARD DEVIATION.

Algorithm 2 Unsupervised Iteration Strategy

Require: input X , threshold t , model \mathcal{F} .

```

1:  $n = 1$ 
2:  $Y^* = 0$ 
3: if  $n < \text{Maxiters}$  then
4:    $P^n = \mathcal{F}(X)$ 
5:   UPDATE  $\mathcal{F}$  with  $Y^*$ 
6:   for  $k \in \{0, 1, \dots, K-1\}$  do
7:      $S_k^n \leftarrow \begin{cases} p = 1 & \text{if } p - t_k > 0, p \in P^n \\ p = 0 & \text{if } p - t_k < 0, p \in P^n \end{cases}$ 
8:   end for
9:    $\tilde{S}^n = \text{argmin}_{k \in \{0, 1, \dots, K-1\}} \text{Cor}(P^n, S_k^n)$ 
10:   $Y^* = S^{\text{meta}} = \text{EMS}(\tilde{S}^n)$ 
11:   $n = n + 1$ 
12: end if

```

the current epoch predictions P^n to generate K coarse segmented images S_k^n ($k = 1, 2, \dots, K$) from K thresholds. The minimum threshold and maximum threshold are the minimum pixels value P_{\min}^n and maximum value P_{\max}^n of P^n , respectively. The interval of neighbor thresholds is $\frac{P_{\max}^n - P_{\min}^n}{K-1}$.

Next, based on an information-theoretic noise-robust loss \mathcal{L}_{DMI} [21], we find the most correlated segmentation image \tilde{S}^n which has the maximum mutual information $\text{Cor}(P^n, S_k^n)$ between P^n and S_k^n ($k = 1, 2, \dots, K$):

$$\text{Cor}(P^n, S_k^n) = \mathcal{L}_{DMI}(P^n, S_k^n) = -\log\left(\left|\det\left(Q_{(P^n \| S_k^n)}\right)\right|\right), \quad (3)$$

where $Q_{(P^n \| S_k^n)}$ is the matrix form of the joint distribution over P^n and S_k^n . To calculate the $Q_{(P^n \| S_k^n)}$, we resize $P^n \in \mathbb{R}^{H \times W}$ to $P_f \in \mathbb{R}^{1 \times HW}$, then concatenate P_f and $1 - P_f$ to $\mathcal{P} \in \mathbb{R}^{2 \times HW}$. Meanwhile, we resize $S_k^n \in \mathbb{R}^{H \times W}$ to $S_f \in \mathbb{R}^{1 \times HW}$, then concatenate S_f and $1 - S_f$ to $\mathcal{S} \in \mathbb{R}^{2 \times HW}$. The $Q_{(P^n \| S_k^n)}$ is defined by matrix multiplication $Q_{(P^n \| S_k^n)} = \mathcal{P}\mathcal{S}^T$.

The optimal \tilde{S}^n that has the maximum $\text{Cor}(P^n, S_k^n)$ then will be sent into an EMS module (i.e., extraction-of-meta-structure module, see section 6.3) to extract the meta-structures S^{meta} . Finally, we update the label Y^* by S^{meta} . The whole iteration strategy is summarized in Algorithm 2. The architecture of iGTT is shown in Appendix D.1.

6.3 Extraction-of-Meta-Structure Module

Because of insufficient training in early training steps, the segmented images \tilde{S}^n by thresholding are extremely coarse. However, the basic topology of objects is largely retained in \tilde{S}^n . Based on this, we design an extraction-of-meta-structure (EMS) module to further improve the quality of pseudo labels.

We first extract the skeleton of \tilde{S}^n , then we randomly shift every pixel in skeleton within a radius r to approximate the width of objects. Since the randomly shift may move some pixel labels outside the target meta-structures, we follow a random sampling operation to filter out these pixel labels and generate the final pseudo label S^{meta} for the next epoch training.

6.4 Segmentation Experiments

As iGTT is customized for binary-class segmentation, we evaluate its performance on the ER, MITO [8] and NUC [42]

datasets. We combine \mathcal{L}_{DMI} and IoU loss function [43] to optimize our models.

To compare with supervised methods, we select U-Net, DeepLabv3+ and a state-of-the-art model HRNet [44]. To compare with unsupervised methods, we select adaptive gaussian thresholding (AGT), Otsu, and two state-of-the-arts methods which including Autoregressive Clustering (AC) [37] and Differentiable Feature Clustering (DFC) [38]. We use DICE (dice scores), AUC (area under curve) and ACC (accuracy) as the performance metrics. To reduce the effects brought by randomization, we trained our model 10 times and calculate the mean and standard deviation.

Segmentation results on ER dataset are summarized in Table 7. Compared to unsupervised methods, iGTT achieves the best performance. Meanwhile, we find that iGTT achieves competitive performance when comparing with the other three supervise models. Moreover, we find that using EMS module improves the final segmentation performance, indicating that EMS indeed refines the candidate labels.

Consistence results are observed on other binary-class datasets. Please see Appendix D.2-4 for details. Overall, our model effectively narrows the gap between supervised learning and unsupervised learning by effectively utilizing meta-structures in noisy labels.

7 THEORETICAL ANALYSIS OF SEMANTICS

In this section, we model meta-structures of labels based on spatial density distributions (SDD) [45]. Then we quantify the semantic of different labels according to meta-structures and propose three theorems to better understand labels in segmentation.

7.1 Preliminaries

Background of Spatial Density Distribution. Spatial density distribution is one of ways to analyze implicit patterns of spatial point data. Kernel density estimation, which is a non-parametric method, estimates the spatial density of events within a specified region by using a kernel function to weight the area surrounding the point according to its distance to the event.

Specifically, for the spatial point data x , the spatial density distributions $f(x)$ can be estimated as follows:

$$f(x) = \frac{1}{2h} \frac{\sum x_i \in [x-h, x+h]}{N} = \frac{1}{2Nh} \sum_{i=1}^N K\left(\frac{x-x_i}{h}\right), \quad (4)$$

where N is the number of data points. h is the bandwidth (radius) of a rectangle search window W , centered at x . K is the kernel function.

Notation. We use M denote the number of semantic classes of uncorrupted image labels \mathcal{Y} . The noisy image labels \mathcal{Y}^* is synthesized by a $M \times M$ $Q_{y^*|y}$. We treat the pixel x^m whose pixel label $y^* = m$ ($y^* \in \mathcal{Y}^*$ and $m \in \{1, 2, \dots, M\}$) as the spatial data point by annotating it as 1 and treat other pixels x^m ($y^* \neq m$) as the background by annotating it as 0. N denotes the number of spatial data points. $f_i(x^m)$ denotes the SDD of semantic class O_i under the spatial data point x^m . We select uniform kernel function K as follows:

$$K(x) = \mathbf{1}(x) = \begin{cases} 1, & |x| \leq 1 \\ 0, & \text{otherwise} \end{cases}. \quad (5)$$

Definition. The meta-structures (MS) of a label are defined as a set of semantic classes O_i , where each O_i is composed of pixels x^m that have similar spatial density $f_i(x^m)$:

$$MS = \{O_1, O_2, \dots, O_M\},$$

$$O_i = \{x^m \mid x^m \sim f_i(x^m)\} \text{ where } (i = 1, 2, \dots, M). \quad (6)$$

Lemma 1: If RCL/RL are synthesized from \mathcal{Y} with $Q_{y^*|y}$, the $f_i(x^m)$ of RCL/RL can be approximated as follows:

$$f_i(x^m) = \frac{1}{2Nh} \sum_{j=1}^M P(y^* = m|y = j) * S_j \pm \delta, \quad (7)$$

where δ denotes the sampling errors that is a constant.

Because N , h , δ and S_j are all constant, $f_i(x^m)$ is only dependent on the flipping probability $P(y^* = m|y = j; j = 1, 2, \dots, M)$.

Proof. By using kernel function K , the $f_i(x^m)$ can be estimated by counting pixels within the search window:

$$f_i(x^m) = \frac{1}{2Nh} \sum_{k=1}^N \mathbf{1}(x-h \leq x_k^m \leq x+h). \quad (8)$$

Note that for RCL and RL, the number of counted pixels within the search window can be approximated by the flipping probability as follows:

$$\sum_{k=1}^N \mathbf{1}(x-h \leq x_k^m \leq x+h) = \sum_{j=1}^M P(y^* = m|y = j) * S_j \pm \delta, \quad (9)$$

where $S_j = W \cap O_j$ is the area that corresponds to j th semantic class O_j within the search area W . Thus, the $f_i(x^m)$ can be approximated as follows:

$$f_i(x^m) = \frac{1}{2Nh} \sum_{j=1}^M P(y^* = m|y = j) * S_j \pm \delta. \quad (10)$$

QED

Lemma 2: The number of semantic classes D of labels equals the rank R of $Q_{y^*|y}$:

$$D = R. \quad (11)$$

Proof. Based on Lemma 1, when the search window of pixel x^m is within area $\{y = i\}$ (i.e., since the search window of near-boundary pixels may contain different semantic objects and these pixels are a minority, we can ignore these pixels for simplify), the $f_i(x^m)$ of semantic class O_i equals:

$$\begin{aligned} f_i(x^m) &= \frac{1}{2Nh} \sum_{j=1}^M P(y^* = m|y = j) * S_j \pm \delta \\ &= \frac{1}{2Nh} * P(y^* = m|y = i) * 4h^2 \pm \delta \\ &= \frac{2h}{N} * P(y^* = m|y = i) \pm \delta. \end{aligned} \quad (12)$$

If rank of $Q_{y^*|y}$ is full $R = M$, there at least exist p and q that $P(y^* = m|y = p) \neq P(y^* = m|y = q), \forall m$. Thus, distribution differences on all semantic classes exist $f_p(x^m) \neq f_q(x^m), \forall p, \forall q$. Based on definition of meta-structures, the number of semantic classes $D = M = R$.

If rank of $Q_{y^*|y}$ is not full $R < M$, there exists $(M - R + 1)$ linearly correlated columns in $Q_{y^*|y}$, indicating for corresponding semantic classes $O_{i,i=1,\dots,M-R+1}$, $P(y^* = m|y = i)$ are equality, $P(y^* = m|y = i) = P_m$. Thus, when the search window of pixel x^m is within area $\{y = 1\} \cup \{y = 2\} \cup \dots \cup \{y = M - R + 1\}$, the $f_{i,i=1,\dots,M-R+1}(x^m)$ equals:

$$f_{i,i=1,\dots,M-R+1}(x^m) = \frac{2hP_m}{N} \pm \delta. \quad (13)$$

This indicates density distributions of $(M - R + 1)$ semantic classes are fused into one. Based on the definition of meta-structures, the number of semantic classes $D = M - (M - R) = R$. In summary, $D = R$. QED

7.2 Quantify Semantics in Labels

Based on Lemma 1 and Lemma 2, we quantify the semantics of different labels.

Semantic of CL and PCL. Since the pixel labels of CL and PCL are unrandomized, their semantic can be directly quantified by calculating SDD from kernel functions:

$$MS(CL) = \{O_1, O_2, \dots, O_M\},$$

$$O_i = \{x^i \mid x^i \sim f_i(x^m)\} \text{ where } i = 1, 2, \dots, M,$$

$$f_i(x^m) = \frac{1}{2Nh} \sum_{k=1}^N \mathbf{1}(x-h \leq x_k^m \leq x+h). \quad (14)$$

Semantic of RCL. For RCL, the $Q_{y^*|y}$ is arbitrary and the

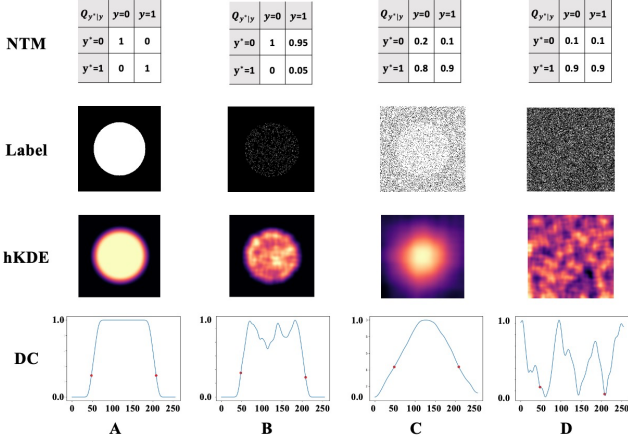


Fig. 10. Spatial density distributions of binary-class semantic labels synthesized by different NTM. The heatmap of kernel density (hKDE) reveals the spatial density of each pixel label in the corresponding location. The density curve (DC) reveals values in the 128th row of hKDE, and the red points denote the location of object outlines in CL.

rank $\in (1, M]$. Thus, the semantic of RCL can be quantified as:

$$MS(RCL) = \{O_1, O_2, \dots, O_M\},$$

$$O_i = \{x^i \mid x^i \sim f_i(x^m)\} \text{ where } 1 < i \leq M,$$

$$f_i(x^m) = \frac{1}{2Nh} \sum_{j=1}^M P(y^* = m \mid y = j) * S_j \pm \delta. \quad (15)$$

Semantic of RL. For RL, the $Q_{y^*|y}$ is arbitrary but the rank equals one. Thus, the semantic of RL can be quantified as:

$$MS(RL) = \{O_1\},$$

$$O_1 = \{x^1 \mid x^1 \sim f_1(x^m)\},$$

$$f_1(x^m) = \frac{1}{2Nh} \sum_{j=1}^M P(y^* = m \mid y = j) * S_j \pm \delta. \quad (16)$$

7.3 Theorems and Proofs

In this section, we proposed three theorems and their corresponding proofs.

Theorem 1: If RCL Y^* is synthesized by $Q_{y^*|y}$ and the rank of $Q_{y^*|y}$ is full, the noisy labels Y^* have similar semantics as CL Y .

Proof. Based on Lemma 2, if $R(Q_{y^*|y}) = M$, the meta-structures of Y^* and the meta-structures of Y have the same number of semantic classes:

$$|MS(Y^*)| = |MS(Y)| = |\{O_1, O_2, \dots, O_M\}| = M. \quad (17)$$

Since the outlines of semantic objects in Y^* are not changed when synthesized from Y , the location of difference between different SDD are also unchanged, indicating that each semantic area of objects in Y^* equals the semantic area of objects in Y . Thus, the meta-structures of Y^* is

TABLE 8
SEGMENTATION PERFORMANCE OF DYNAMIC RCLs

Dataset	Model	CL	Dynamic RCL
ER	U-Net	75.4	74.8
MITO	U-Net	67.8	67.1
Cityscapes	DeepLabv3+	64.8	64.2
Cityscapes-3	DeepLabv3+	94.3	93.9

identical to the meta-structures of Y , and they have the similar semantics. *QED*

We also demonstrate Theorem 1 by experiments. We simulate a simplified binary-class CL of (256×256) that has a circle within a rectangle as shown in Fig.9a. We synthesized RCLs with different $Q_{y^*|y}$ as shown in Fig.9b-e and RLs as shown in Fig.9f.

The SDD of labels are visualized in two ways: heatmaps of kernel density estimation (hKDE) and density curves (DC). The hKDE directly reveals spatial density of each pixel label in corresponding location. The DC reveals values in the 128th row of hKDE, and the red points denote the location of semantic object outlines in CL.

Fig.9a shows the hKDE and DC of the CL. The hKDE clearly shows the difference of SDD between two semantic classes and the high-density values are aggregated in the circular region (foreground). Meanwhile, we can see the large changing rates nearby the location of object outlines in DC. Both hKDE and DC reveal that meta-structures of CL contain two semantic classes and each of them consists of pixels that have similar density distributions.

For the RCL whose rank of $Q_{y^*|y}$ equals 2 (Fig.9b-e), all of their hKDE and DC have similar density differences as CL between the foreground and the background, indicating that RCL contain similar meta-structures as CL.

However, for the RL that rank of $Q_{y^*|y}$ equals 1 (Fig.9f), the hKDE and DC are randomization. Two density distributions are fused into one, indicating the decreases of semantic.

We can achieve consistent results on multi-class semantic labels after divided labels into multiple binary-class semantic labels. The detailed experiments are shown in Appendix E.

Theorem 2: For PCL Y^* , more un-randomized pixel biases on CL Y , more perturbation on semantic.

Proof. As shown in Fig.2, the semantic area D of PCL can be divided into two components, unperturbed area D' and perturbed area P :

$$D = D' + P. \quad (18)$$

Based on Lemma 2, within D' , the $Q_{y^*|y}$ is an identity matrix, indicating no semantic changes. Within P , the $Q_{y^*|y}$ is a matrix which rank equals 1, indicating semantic changes in this area. Thus more bias on CL will lead increasing area of P , indicating more perturbation on semantic. *QED*

Theorem 3: If optimization is based on empirical risk minimization (ERM) [9], when DNNs trained by *dynamic*

full-rank RCL, which means we randomly synthesized RCL with different full-rank NTM Q in each training epoch, DNNs still have similar performance as it trained by CL.

Proof: For dynamic RCL, the empirical risk $R(f)$ can be denoted as the expectation of loss function under random variable Q :

$$R(f) = \mathbb{E}_Q[L(f(x), y_Q)] = \sum_Q P(Q) * \mathcal{L}(f(x), y_Q), \quad (19)$$

where f denotes the learning systems, L denotes the loss function, $P(Q)$ denotes the probability of Q . Based on the Law of Large Numbers [46], we have:

$$R(f) = \lim_{n \rightarrow \infty} \frac{1}{n} \sum_{i=1}^n \mathcal{L}(f(x), y_{Q_i}). \quad (20)$$

Thus minimize $R(f)$ can be converted to minimize each $\mathcal{L}(f(x), y_{Q_i})$ independently. If $f_i = \operatorname{argmin} \mathcal{L}(f(x), y_{Q_i})$, we have:

$$f^* = \operatorname{argmin} R(f) = \lim_{n \rightarrow \infty} \frac{1}{n} \sum_{i=1}^n f_i. \quad (21)$$

This indicates that f^* optimized by dynamic RCL can be viewed as the boosting of a series of f_i , where each f_i is trained by RCL with the fixed full-rank NTM Q_i .

Since DNNs trained by RCL with fixed full-rank Q_i have similar performance as DNNs trained by CL (*Theorem 1*), the DNNs trained by dynamic RCL will have similar performance. *QED*

We also demonstrate *Theorem 3* by experiments. In each epoch of training, we dynamically synthesized RCL with different full-rank $Q_{y^*|y}$ for all labels. The segmentation results on four datasets are shown in Table 8. As we can see, the DNNs trained by dynamic RCL achieve the competitive segmentation performance as the DNNs trained by CL.

Summary

Theorem 1 demonstrates that RCL with full rank of $Q_{y^*|y}$ contain similar semantics as CL. This explains why DNNs trained by RCL have similar performance as DNNs trained CL.

Theorem 2 demonstrates that the semantics of PCL are essentially different from CL since their components of semantic classes are different. This explains why PCL degrades performance in both of feature extraction and segmentation.

Theorem 3 demonstrates that noisy-free on pixel labels is not the only golden standard for training DNNs.

7 CONCLUSION

In this study, we examine the learning behavior of DNNs trained by different types of pixel-level noisy labels in semantic segmentation and provide direct experimental evidence and theoretical proof that DNNs learn meta-structures from noisy labels. The unsupervised segmentation

model we have developed provides an example on how to utilize the meta-structures in practice. However, our study also has its limitations. In particular, our model of meta-structures remains to be further developed, and utilization of meta-structures remains to be expanded to other applications such as multi-class segmentation. Despite these limitations, the learning behavior of DNNs revealed in this study provides new insight into what and how DNNs learn from noisy labels to segment images.

ACKNOWLEDGMENT

The authors thank members of CBMI for their technical assistance. The work was supported in part by the National Natural Science Foundation of China (grant 31971289 and 91954201 to G.Y.) and the Strategic Priority Research Program of the Chinese Academy of Sciences (grant XDB37040402 to G.Y.).

REFERENCES

- [1] M.H. Hesamian, W. Jia, X. He, and P. Kennedy, "Deep Learning Techniques for Medical Image Segmentation: Achievements and Challenges," *Journal of Digital Imaging*, vol. 32, no. 4, pp. 582-596, 2019.
- [2] S. Minaee, Y.Y. Boykov, F. Porikli, A.J. Plaza, N. Kehtarnavaz, and D. Terzopoulos, "Image Segmentation Using Deep Learning: A Survey," *IEEE Transactions on Pattern Analysis and Machine Intelligence*, pp. 1-1, 2021.
- [3] A. Garcia-Garcia, S. Orts-Escobedo, S. Oprea, V. Villena-Martinez, P. Martinez-Gonzalez, and J. Garcia-Rodriguez, "A survey on deep learning techniques for image and video semantic segmentation," *Applied Soft Computing*, vol. 70, pp. 41-65, 2018.
- [4] D. Arpit, S. Jastrzebski, N. Ballas, D. Krueger, E. Bengio, M.S. Kanwal, T. Maharaj, A. Fischer, A. Courville, and Y. Bengio, "A closer look at memorization in deep networks," in *Proc. Int. Conf. Mach. Learn.*, 2017, pp. 233-242.
- [5] C. Zhang, S. Bengio, M. Hardt, B. Recht, and O. Vinyals, "Understanding deep learning (still) requires rethinking generalization," *Commun. ACM*, vol. 64, no. 3, pp. 107-115, 2021.
- [6] O. Ronneberger, P. Fischer, and T. Brox, "U-net: Convolutional networks for biomedical image segmentation," in *Proc. Int. Conf. Med. Image Comput. Comput.-Assisted Interv.*, 2015, pp. 234-241.
- [7] L.-C. Chen, Y. Zhu, G. Papandreou, F. Schroff, and H. Adam, "Encoder-decoder with atrous separable convolution for semantic image segmentation," in *Proc. Eur. Conf. Comput. Vis.*, 2018, pp. 801-818.
- [8] Y. Luo, Y. Guo, W. Li, G. Liu, and G. Yang, "Fluorescence Microscopy Image Datasets for Deep Learning Segmentation of Intracellular Organelle Networks," *IEEE Dataport*, 2020.
- [9] V. Vapnik, "Principles of risk minimization for learning theory," in *Proc. Adv. Neural Inf. Process. Syst.*, 1992, pp. 831-838.
- [10] P. Chen, B.B. Liao, G. Chen, and S. Zhang, "Understanding and utilizing deep neural networks trained with noisy labels," in *Proc. Int. Conf. Mach. Learn.*, 2019, pp. 1062-1070.
- [11] A. Xu, and M. Raginsky, "Information-theoretic analysis of

- generalization capability of learning algorithms," *Proc. Adv. Neural Inf. Process. Syst.*, vol. 30, 2017.
- [12] H. Harutyunyan, K. Reing, G. Ver Steeg, and A. Galstyan, "Improving generalization by controlling label-noise information in neural network weights," in *Proc. Int. Conf. Mach. Learn.*, 2020, pp. 4071-4081.
- [13] L. Jaehwan, Y. Donggeun, and K. Hyo-Eun, "Photometric transformer networks and label adjustment for breast density prediction," in *Proc. IEEE Int. Conf. Comput. Vis. workshops*, 2019, pp. 0-0.
- [14] B. Yuan, J. Chen, W. Zhang, H.-S. Tai, and S. McMains, "Iterative cross learning on noisy labels," in *IEEE Winter Conf. Appl. Comput. Vis.*, 2018, pp. 757-765.
- [15] J. Krause, B. Sapp, A. Howard, H. Zhou, A. Toshev, T. Duerig, J. Philbin, and L. Fei-Fei, "The unreasonable effectiveness of noisy data for fine-grained recognition," in *Proc. Eur. Conf. Comput. Vis.*, 2016, pp. 301-320.
- [16] J.P. Brooks, "Support vector machines with the ramp loss and the hard margin loss," *Oper Res*, vol. 59, no. 2, pp. 467-479, 2011.
- [17] N. Manwani, and P. Sastry, "Noise tolerance under risk minimization," *IEEE Trans Cybern*, vol. 43, no. 3, pp. 1146-1151, 2013.
- [18] H. Masnadi-Shirazi, and N. Vasconcelos, "On the design of loss functions for classification: theory, robustness to outliers, and savageboost," *Proc. Adv. Neural Inf. Process. Syst.*, vol. 21, 2008.
- [19] B. Van Rooyen, A. Menon, and R.C. Williamson, "Learning with symmetric label noise: The importance of being unhinged," *Proc. Adv. Neural Inf. Process. Syst.*, vol. 28, 2015.
- [20] A. Ghosh, H. Kumar, and P. Sastry, "Robust loss functions under label noise for deep neural networks," in *Proc. AAAI Conf. Artif. Intell.*, 2017.
- [21] Y. Xu, P. Cao, Y. Kong, and Y. Wang, "L_DMI: A Novel Information-theoretic Loss Function for Training Deep Nets Robust to Label Noise," in *Proc. Adv. Neural Inf. Process. Syst.*, 2019, pp. 6222-6233.
- [22] Z. Zhang, and M.R. Sabuncu, "Generalized cross entropy loss for training deep neural networks with noisy labels," in *Proc. Adv. Neural Inf. Process. Syst.*, 2018.
- [23] B. Han, Q. Yao, X. Yu, G. Niu, M. Xu, W. Hu, I. Tsang, and M. Sugiyama, "Co-teaching: Robust training of deep neural networks with extremely noisy labels," *Proc. Adv. Neural Inf. Process. Syst.*, vol. 31, 2018.
- [24] L. Jiang, Z. Zhou, T. Leung, L.-J. Li, and L. Fei-Fei, "Mentornet: Learning data-driven curriculum for very deep neural networks on corrupted labels," in *Proc. Int. Conf. Mach. Learn.*, 2018, pp. 2304-2313.
- [25] J. Li, R. Socher, and S.C. Hoi, "Dividemix: Learning with noisy labels as semi-supervised learning," *arXiv:2002.07394*, 2020.
- [26] D. Tanaka, D. Ikami, T. Yamasaki, and K. Aizawa, "Joint optimization framework for learning with noisy labels," in *Proc. IEEE Conf. Comput. Vis. Pattern Recognit.*, 2018, pp. 5552-5560.
- [27] A. Veit, N. Alldrin, G. Chechik, I. Krasin, A. Gupta, and S. Belongie, "Learning from noisy large-scale datasets with minimal supervision," in *Proc. IEEE Conf. Comput. Vis. Pattern Recognit.*, 2017, pp. 839-847.
- [28] S. Min, X. Chen, Z.-J. Zha, F. Wu, and Y. Zhang, "A two-stream mutual attention network for semi-supervised biomedical segmentation with noisy labels," in *Proc. AAAI Conf. Artif. Intell.*, 2019, pp. 4578-4585.
- [29] Y. Shu, X. Wu, and W. Li, "Lvc-net: Medical image segmentation with noisy label based on local visual cues," in *Proc. Int. Conf. Med. Image Comput. Comput.-Assisted Interv.*, 2019, pp. 558-566.
- [30] Y. Li, L. Jia, Z. Wang, Y. Qian, and H. Qiao, "Un-supervised and semi-supervised hand segmentation in egocentric images with noisy label learning," *Neurocomputing*, vol. 334, pp. 11-24, 2019.
- [31] Z. Lu, Z. Fu, T. Xiang, P. Han, L. Wang, and X. Gao, "Learning from weak and noisy labels for semantic segmentation," *IEEE Trans. Pattern Anal. Mach. Intell.*, vol. 39, no. 3, pp. 486-500, 2016.
- [32] S. Navlakha, P. Ahammad, and E.W. Myers, "Unsupervised segmentation of noisy electron microscopy images using salient watersheds and region merging," *BMC Bioinform.*, vol. 14, no. 1, pp. 1-9, 2013.
- [33] Z. Zheng, and Y. Yang, "Rectifying pseudo label learning via uncertainty estimation for domain adaptive semantic segmentation," *Int. J. Comput. Vis.*, vol. 129, no. 4, pp. 1106-1120, 2021.
- [34] J.-J. Hwang, S.X. Yu, J. Shi, M.D. Collins, T.-J. Yang, X. Zhang, and L.-C. Chen, "Segsort: Segmentation by discriminative sorting of segments," in *Proc. IEEE Int. Conf. Comput. Vis.*, 2019, pp. 7334-7344.
- [35] X. Zhang, and M. Maire, "Self-supervised visual representation learning from hierarchical grouping," *Proc. Adv. Neural Inf. Process. Syst.*, vol. 33, pp. 16579-16590, 2020.
- [36] X. Ji, J.F. Henriques, and A. Vedaldi, "Invariant information clustering for unsupervised image classification and segmentation," in *Proc. IEEE Int. Conf. Comput. Vis.*, 2019, pp. 9865-9874.
- [37] Y. Ouali, C. Hudelot, and M. Tami, "Autoregressive unsupervised image segmentation," in *Proc. Eur. Conf. Comput. Vis.*, 2020, pp. 142-158.
- [38] W. Kim, A. Kanazaki, and M. Tanaka, "Unsupervised learning of image segmentation based on differentiable feature clustering," *IEEE Trans Image Process*, vol. 29, pp. 8055-8068, 2020.
- [39] D. Angluin, and P. Laird, "Learning from noisy examples," *Machine Learning*, vol. 2, no. 4, pp. 343-370, 1988.
- [40] M. Cordts, M. Omran, S. Ramos, T. Rehfeld, M. Enzweiler, R. Benenson, U. Franke, S. Roth, and B. Schiele, "The cityscapes dataset for semantic urban scene understanding," in *Proc. IEEE Conf. Comput. Vis. Pattern Recognit.*, 2016, pp. 3213-3223.
- [41] D. Erhan, Y. Bengio, A. Courville, and P. Vincent, "Visualizing higher-layer features of a deep network," vol. 1341, no. 3, pp. 1, 2009.
- [42] J.C. Caicedo, A. Goodman, K.W. Karhohs, B.A. Cimini, J. Ackerman, M. Haghighi, C. Heng, T. Becker, M. Doan, and C. McQuin, "Nucleus segmentation across imaging experiments: the 2018 Data Science Bowl," *Nat. Methods*, vol. 16, no. 12, pp. 1247-1253, 2019.
- [43] Y. Huang, Z. Tang, D. Chen, K. Su, and C. Chen, "Batching soft IoU for training semantic segmentation networks," *IEEE Signal Process Lett*, vol. 27, pp. 66-70, 2019.
- [44] J. Wang, K. Sun, T. Cheng, B. Jiang, C. Deng, Y. Zhao, D. Liu, Y. Mu, M. Tan, and X. Wang, "Deep high-resolution representation

learning for visual recognition,” *IEEE Trans. Pattern Anal. Mach. Intell.*, vol. 43, no. 10, pp. 3349-3364, 2020.

[45] A. Baddeley, E. Rubak, and R. Turner, *Spatial point patterns: methodology and applications with R*: CRC press, 2015.

[46] P.-L. Hsu, and H. Robbins, “Complete convergence and the law of large numbers,” vol. 33, no. 2, pp. 25, 1947.